Nanotechnology

PAPER

High mobility field-effect transistors based on MoS_2 crystals grown by the flux method

To cite this article: Vilas Patil *et al* 2021 *Nanotechnology* **32** 325603

IOP Publishing Nanotechnology
Nanotechnology 32 (2021) 325603 (9pp) https://doi.org/10.1088/1361-6528/abf6f1

High mobility field-effect transistors based on MoS_2 crystals grown by the flux method

Vilas Patil[1,2], Jihyun Kim[3], Khushabu Agrawal[1], Tuson Park[3], Junsin Yi[1], Nobuyuki Aoki[4], Kenji Watanabe[5], Takashi Taniguchi[6] and Gil-Ho Kim[1,7,*]

[1] School of Electronic and Electrical Engineering, Sungkyunkwan University (SKKU), Suwon 16419, Republic of Korea
[2] Department of Condensed Matter Physics and Materials Science, Tata Institute of Fundamental Research, Homi Bhabha Road, Mumbai 400005, India
[3] Centre for Quantum Materials and Superconductivity (CQMS), Department of Physics, Sungkyunkwan University, Suwon 16419, Republic of Korea
[4] Department of Materials Science, Chiba University, Chiba 263-8522, Japan
[5] Research Centre for Functional Materials, National Institute for Materials Science, 1-1 Namiki, Tsukuba 305-0044, Japan
[6] International Centre for Materials Nano-Architectonics, National Institute for Materials Science, 1-1 Namiki, Tsukuba 305-0044, Japan
[7] Sungkyunkwan Advanced Institute of Nanotechnology (SAINT), Sungkyunkwan University, Suwon 16419, Republic of Korea

E-mail: tp8701@skku.edu and ghkim@skku.edu

Received 18 December 2020, revised 30 March 2021
Accepted for publication 12 April 2021
Published 17 May 2021

Abstract

Two-dimensional (2D) molybdenum disulphide (MoS_2) transition metal dichalcogenides (TMDs) have great potential for use in optical and electronic device applications; however, the performance of MoS_2 is limited by its crystal quality, which serves as a measure of the defects and grain boundaries in the grown material. Therefore, the high-quality growth of MoS_2 crystals continues to be a critical issue. In this context, we propose the formation of high-quality MoS_2 crystals via the flux method. The resulting electrical properties demonstrate the significant impact of crystal morphology on the performance of MoS_2 field-effect transistors. MoS_2 made with a relatively higher concentration of sulphur (a molar ratio of 2.2) and at a cooling rate of 2.5 °C h^{-1} yielded good quality and optimally sized crystals. The room-temperature and low-temperature (77 K) electrical transport properties of MoS_2 field-effect transistors (FETs) were studied in detail, with and without the use of a hexagonal boron nitride (h-BN) dielectric to address the mobility degradation issue due to scattering at the SiO_2/2D material interface. A maximum field-effect mobility of 113 $cm^2 V^{-1} s^{-1}$ was achieved at 77 K for the MoS_2/h-BN FET following high-quality crystal formation by the flux method. Our results confirm the achievement of large-scale high-quality crystal growth with reduced defect density using the flux method and are key to achieving higher mobility in MoS_2 FET devices in parallel with commercially accessible MoS_2 crystals.

Keywords: MoS_2, Flux method, Field-effect transistor, hexagonal boron nitride (h-BN)

(Some figures may appear in colour only in the online journal)

1. Introduction

Over the last two decades, transition metal dichalcogenides (TMDs) have been a focal point, owing to their potential application in next-generation electronic and optoelectronic

* Author to whom any correspondence should be addressed.

Table 1. Process parameters of high-quality crystal MoS_2 growth via the flux method.

		Material Molar Ratio			
		Cooling rate: 2.5 °C h^{-1}		Cooling rate: 2 °C h^{-1}	
Material	Purity	Sample #1	Sample #2	Sample #3	Sample #4
Mo	4N	1	1	1	1
S	5N	2	2.2	2	2.2
Sn	5N	15	15	15	15

devices. One of these TMDs is 2D MoS_2, which consists of covalently coupled S-Mo-S (sulphur-molybdenum-sulphur) sheets with weak van der Waals forces between them. The MoS_2 bandgap ranges from 1.2 eV (bulk) to 1.8 eV (single layer), depending on the number of coupled layers, allowing different applications [1, 2]. However, certain challenges need to be addressed before MoS_2 can be used in actual device applications. One of these challenges is the crystal quality of grown MoS_2, which is an important factor in the production of electronic devices with respect to performance [3, 4]. The crystal quality, number of layers, and the chemical composition are factors that could degrade the fabricated device performance. Therefore, crystal growth techniques play an important role in determining the crystal quality and hence the device performance [5].

Good quality MoS_2 crystals can be obtained via vapor deposition techniques such as chemical vapor deposition (CVD), chemical vapor transport (CVT), pulsed laser deposition (PLD), or other chemical synthesis routes. There are many reports of the successful growth of MoS_2 crystals by CVD, CVT, and PLD [6–9]. The crystal quality appears to be dependent on parameters such as growth temperature, precursor concentration, gas-flow rates, and the growth pressure of the furnace. Regardless of the success of CVD, issues such as tensile stress due to substrate interaction and by-products of a possible loss of reaction result in impurities in the grown MoS_2 layers. This leads to disadvantages such as cracks and grain boundaries in the material, resulting in intrinsic rippling in the layered regions [10–13]. Recently, the flux method has gained attention for yielding high-quality, defect-free, large-area 2D crystals. The flux method is a solution-based growth technique, whereby the required material is dissolved in a solvent (flux). The grown crystals are free from thermal strain, and the desired quality of crystals can be obtained by optimizing the process temperature. 2D crystals grown by the flux method possess a defect density that is one to two orders lower than that of commercially available crystal materials [14]. Zhang *et al* [15] reported the growth of MoS_2 crystals using a tin (Sn) flux and explored its use for photonic applications. Cevallos *et al* [16] used a common salt flux to grow MoS_2 and WS_2 layered crystals and obtained excellent photoluminescent properties. Furthermore, flux-grown MoS_2 crystals can also be utilised for solar cells [17], photoluminescence [18], and various frequency-generation [19] applications.

Although the MoS_2 crystals grown via the flux method retain excellent optical properties, the desired electrical properties have not yet been studied. In addition, the 2D material properties are highly reliant on the supporting dielectric substrate used in the device fabrication. SiO_2 has been a popular choice of dielectric for device fabrication, due to its ideal interface properties when used with Si. However, 2D layers exfoliated on SiO_2 tend to suffer from mobility degradation due to carrier scattering and trapped charges at the SiO_2/2D layer interface [20]. To address this problem, the use of hexagonal boron nitride (h-BN) layers has been proposed by various groups in recent studies [21, 22]. An h-BN substrate is an excellent support for the exfoliated MoS_2, improving device performance in terms of mobility. In this study, we report the electrical properties of high-quality MoS_2 crystals grown using the flux method and mechanically exfoliated for device applications with and without h-BN. This study aims to elucidate the relationship between the cooling rate and molar ratio in MoS_2 crystals and their electrical mobility. This study reveals that the cooling rate has a significant impact on the material's mobility, which is strongly related to crystal size and quality. We prepared four different ampules: the first two ampules had a 1:2:15 molar ratio and the other two had 1:2.2:15 molar ratios. Afterwards, two different molar ratio ampules were prepared at a 2.5 °C h^{-1} cooling rate and the other two were prepared at 2.0 °C h^{-1}. The grown MoS_2 flux was characterized by x-ray diffraction (XRD) and Raman spectroscopy. The high-quality flux-grown MoS_2 crystals mechanically exfoliated on an h-BN dielectric showed great improvement in mobility, compared to that of a non-h-BN layer device measured at 10^{-3} Torr of pressure.

2. Experimental details

2.1. MoS_2 crystal growth by flux method

To grow high-quality crystals, the method reported by Zhang *et al* [15] was adopted. Here, we used a Sn flux, and Sn did not contribute to the reaction because it is an unreactive solvent. It has a lower melting point than sulphur (S) and molybdenum (Mo), and it also remains stable during the high-temperature process allowing the formation of MoS_2, preventing impurities from being added. It is also easy to remove or clean after the formation of MoS_2 crystals [16]. The four different samples were prepared with two different molar ratios and different cooling rates. Table 1 gives the details for all four samples. To check whether it was possible to

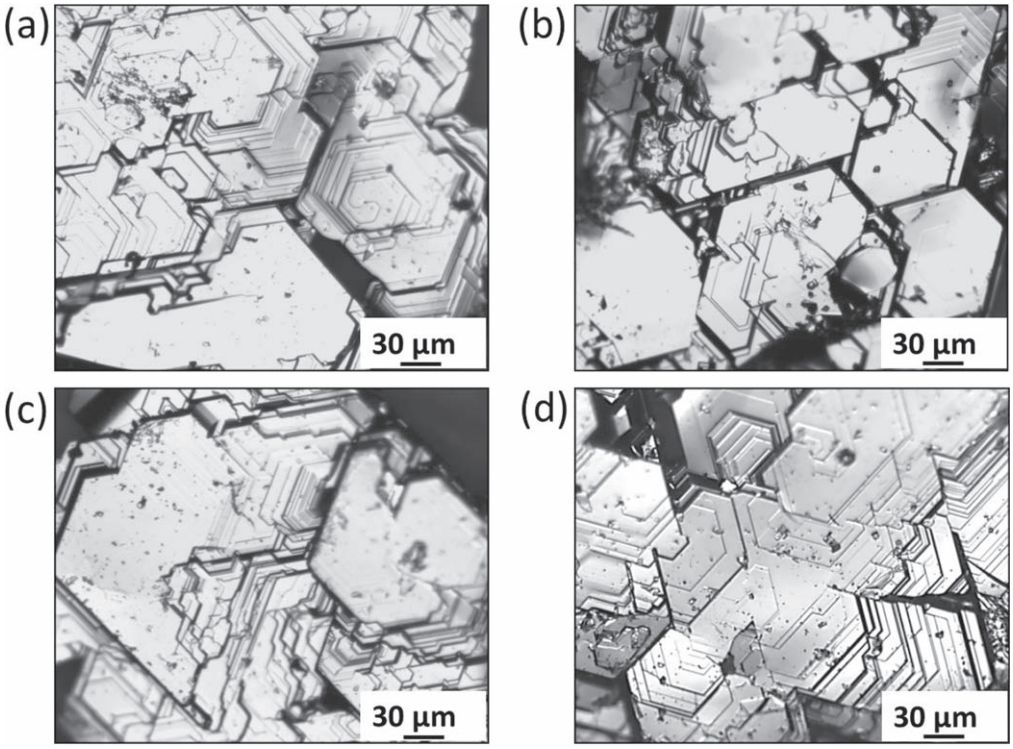

Figure 1. Microscopic images of MoS_2 crystals grown by the flux method (a) with a molar ratio of 1:2:15 and a cooling rate of 2.5 °C h^{-1} (b) a molar ratio of 1:2.2:15 and a cooling rate of 2.5 °C h^{-1} (c) a molar ratio of 1:2:15 and a cooling rate of 2 °C h^{-1} (d) a molar ratio of 1:2.2:15 and a cooling rate of 2 °C h^{-1}. Image (b) shows the clear formation of large crystals.

overcome sulphur vacancies in the MoS_2 crystals, one sample was prepared with a high sulphur concentration.

The source materials were added into an alumina crucible fixed into a quartz tube ampule, which was later vacuum sealed and loaded into a high-temperature furnace at 1100 °C at a ramp-up rate of 50 °C h^{-1}. The temperature was held constant for 48 h and then the samples were allowed to cool down at 2.5 °C h^{-1} and 2 °C h^{-1}, respectively. The resultant ampules were centrifuged at 2000 rpm for 60 s. The grown crystals were characterized by Raman spectroscopy and x-ray diffraction techniques to verify the crystal formation and crystal quality. The formed crystals were then used for device fabrication.

2.2. Device fabrication and characterization

Four different devices with the same number of 2D layers (six layers) were fabricated via mechanical exfoliation of the flux-grown crystal to obtain MoS_2 crystals on a (285 nm) SiO_2/Si substrate. The substrate was precleaned with acetone and isopropyl alcohol (IPA) before mechanical exfoliation. Exfoliated MoS_2 flakes were then transferred onto the h-BN/SiO_2/Si substrate using the dry transfer poly-dimethylsiloxane, and polycarbonate (PDMS and PC stamp) method. The source and drain electrodes were patterned through a standard photolithographic process. Au/In (10/30 nm) bilayer metal electrodes were deposited using the e-beam evaporation technique. A lift-off process was carried out to remove unwanted metal and photoresist from the sample. Finally, the device was subjected to post-metallization annealing at 120 °C for 90 min in an argon gas atmosphere to enhance the contact properties. Figure 2(a) shows a typical schematic of the fabricated device structure. After verifying the crystal quality of all four samples, a device with a few layers of h-BN used as a dielectric between the SiO_2 and the MoS_2 was fabricated, using similar process parameters for fabrication to those given above.

The flux-grown MoS_2 crystals exfoliated onto Si/SiO_2 substrates were visualised using an Olympus BX51 optical microscope at a resolution of 20 μm. A Renishaw confocal Raman spectrometer with a monochromatic laser source with a wavelength of 514.5 nm was used to characterize the molecular vibrations in the six-layer MoS_2 flake. The crystal quality was examined using a Bruker Advance D8 x-ray diffractometer at various angular settings between 5° and 85°. The electrical characteristics such as the I_{ds}-V_{gs} and I_{ds}-V_{ds} of all five devices with and without the h-BN were investigated by measuring the device at room temperature (RT) and at 77 K using a Keithley-4200 interactive test module. All the electrical measurements were performed in a vacuum environment at a pressure of 2×10^{-3} Torr.

3. Results and discussion

Optical images of MoS_2 crystals grown under different conditions are shown in figures 1(a)–(d). Figure 1 intimates that the cooling rate has a significant impact on crystal morphology.

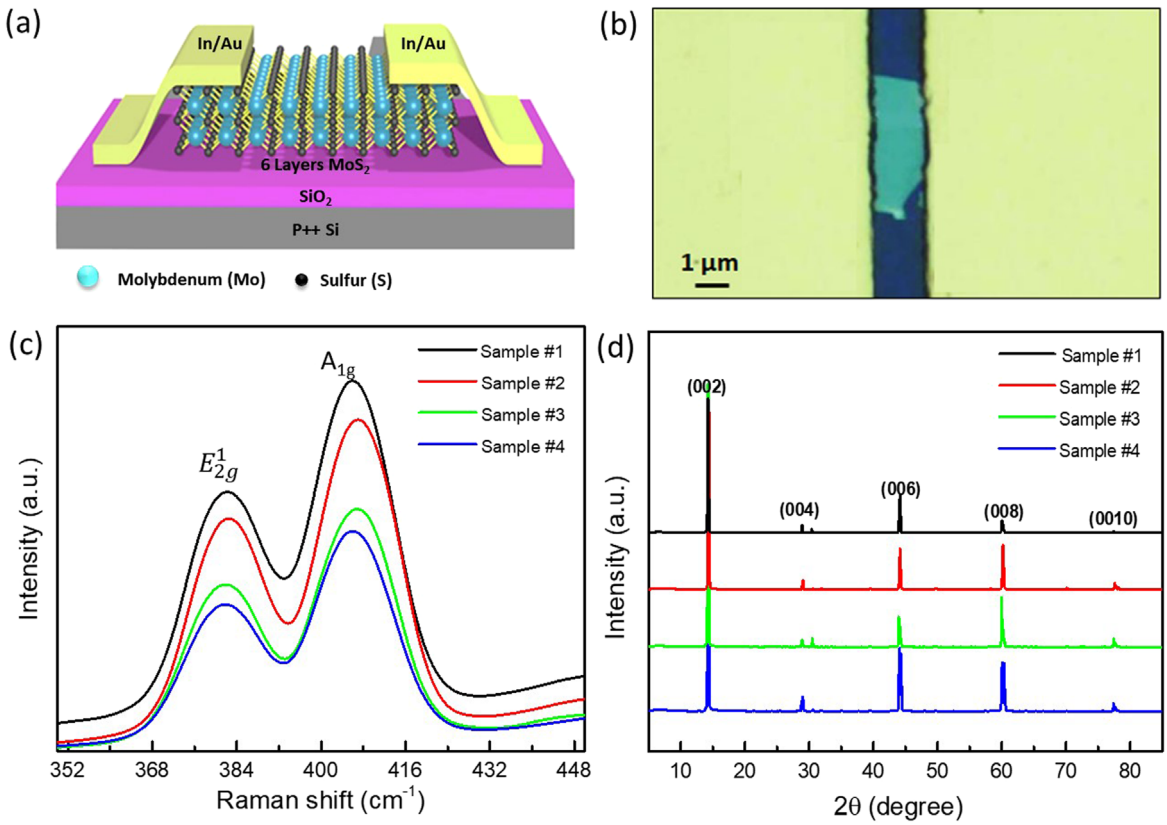

Figure 2. (a) A 3D schematic of the six-layer MoS_2 device with In/Au metal contacts fabricated on 285 nm of SiO_2/Si. (b) Optical image of the real device. (c) Raman spectrum of six-layer MoS_2 crystals grown under four different sets of conditions via the flux method at room temperature. (d) XRD pattern of a 2H-MoS_2 high-quality single crystal formed under four different sets of conditions. Sample #1. 1:2:15, 2.5 °C h^{-1}; sample #2. 1:2.2:15, 2.5 °C h^{-1}; sample #3. 1:2:15, 2 °C h^{-1}; and sample #4. 1:2.2:15, 2 °C h^{-1}.

Figure 1(a) is an optical image of the crystal formed at a 2.5 °C h^{-1} cooling rate with a sulphur to molybdenum ratio of 2:1. Cracks in the crystal were observed at lower molar sulphur concentrations. Figure 1(b) shows high-quality MoS_2 single crystals in the sample for which the cooling rate was maintained at 2.5 °C h^{-1} and which had 1:2.2:15 molar ratios of Mo, S, and Sn, respectively. Furthermore, the cooling rate was decreased to 2.0 °C h^{-1} and with similar sulphur concentrations, as above. Figure 1(c) shows that lower-quality crystal formation tends towards the polycrystalline phase with 1:2:15 molar ratios. We further increased the sulphur molar ratio to 2.2, resulting in good quality crystals at a cooling rate of 2.0 °C h^{-1}, as shown in figure 1(d). The optical images show the formation of crystalline MoS_2 crystals grown in the Sn flux with a greater decrease in the cooling rate. The crystals obtained were later used to investigate the effects of crystal morphology on the optical and electrical properties of MoS_2 FETs.

Raman spectroscopy was used to verify the formation of six-layer single-crystal MoS_2 over SiO_2/Si. A high-resolution Raman microscope was used to measure the Raman shift in the grown samples at an excitation wavelength (λ_{ex}) of 532 nm. Figure 2(c) shows the Raman spectra for all four samples grown by the flux method. The two sharp peaks at 406.8 cm^{-1} and 382.18 cm^{-1} correspond to the A_{1g} active mode and the E^1_{2g} vibrational modes. The A_{1g} mode is related to the in-plane vibration of the S atoms, while E^1_{2g} suggests the out-of-plane vibration of the Mo and S atoms. The peak separation of 24.5 cm^{-1} is the same for all samples, demonstrating that the number of layers is six for each device [23]. Furthermore, the peak intensity is observed to decrease as the crystal size increases, indicating the large crystal formation of sample 4. The Raman peak intensity is also used to demonstrate the surface adsorptions and surface functionalization conditions describing the optical transitions at different excitation energies [24, 25]. The peak intensity is dependent on the excitation energy used during measurement. A higher excitation energy can lead to a higher peak intensity; however, the E_{2g} mode always has a lower intensity than the A_{1g} mode, as it is dependent on the A_{1g} close to the C excitation energy band, which is found to be similar here for the case of MoS_2 crystals grown by the flux method.

Furthermore, the decrease in the A_{1g} and E^1_{2g} peak intensities attributed to the structural changes between the interlayers, the lattice vibration due to variation in the cooling rate and the sulphur content during the growth of MoS_2 flakes, and the mechanical exfoliation would not cause the change in the intensity of the Raman peak.

The x-ray diffraction (XRD) pattern in figure 2(d) shows single-crystal 2H MoS_2 peaks for all four samples. The 2θ peaks at 14.2°, 29.1°, 44.2°, 60.2°, and 77.5° correspond to the (002), (004), (006), (008), and (0010) planes of the MoS_2

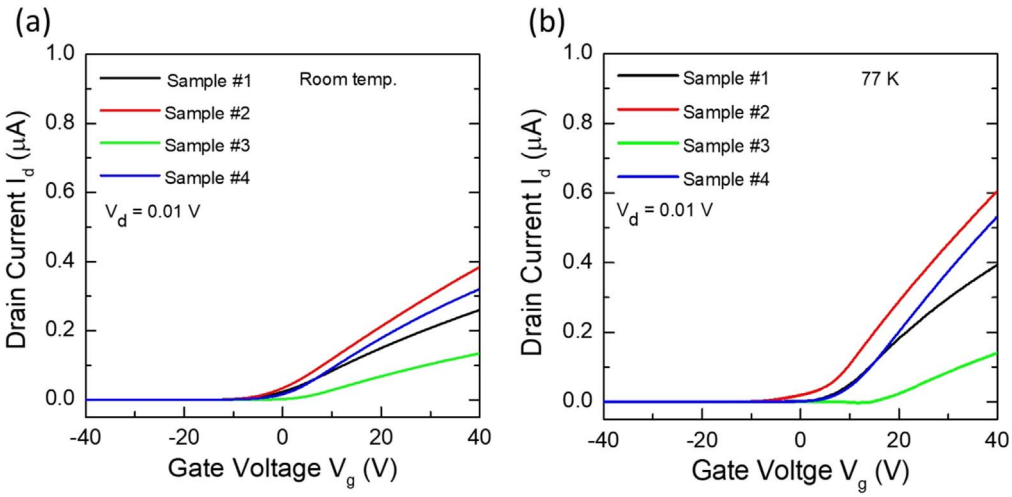

Figure 3. Electrical properties of the MoS_2 FET. (a) Transfer characteristics of the four different devices measured at room temperature with $V_{ds} = 0.01$ V and back-gate voltages varying from −40 V to 40 V. (b) Low-temperature transfer characteristics of the MoS_2 FET measured at 77 K with $V_{ds} = 0.01$ V and gate voltages ranging −40 to 40 V. All measurements were carried out at 2×10^{-3} Torr pressure.

hexagonal structure, respectively, and these results are consistent with those of the Joint Committee on Powder Diffraction Standards *(JCPDS)* card no. 37-1492. The (00l) diffraction plane, attributed to a d-spacing of 0.62 nm, was observed for a single-crystal MoS_2 flake [26]. Further, the additional peak at approximately 30.59° in samples 1 and 3 is related to the presence of defects, while the shift to lower angles for the sulphur peak at 31.40° gives an increase in interlayer spacing from 0.28 to 0.29 nm [27]. However, this peak is insignificant in the XRD spectra of samples 2 and 4 because of the additional sulphur molar concentration, which therefore helps to overcome these defects. In the crystal structure of materials, the ab-plane strongly shows the two-dimensional growth behaviour of MoS_2 for samples 2 and 4, matching the similar behaviour for high-quality crystal growth results reported by Zhang *et al* [15]. Therefore, we can consider the MoS_2 crystals grown via the Sn flux method described in this study to be high-quality single crystals.

Figure 3 shows the transfer characteristics (I_{ds} versus V_{gs}) of the non-h-BN MoS_2 field-effect transistors measured at RT (a) and 77 K (b) at a small applied drain voltage (V_{ds}) of 0.01V for four different crystals. All four devices show an linear increment in the drain current with respect to the gate voltage, and n-type conductive behaviour. Among them, the devices with higher sulphur concentrations of 2.2 M exhibit an improvement in the drain current, as observed in figures 3(a) and (b) measured at RT and 77 K, respectively, except for sample 3 at 77 K, which shows a reduction in the drain current. The possibility is undeniable that sulphur vacancies are present, which later become a source of grain boundaries in the exfoliated samples, as reported by various groups through scanning tunnelling microscopy [14]. The introduction of O_2 or H_2 annealing can heal this vacancy, as reported earlier [28–30].

However, the extra sulphur concentration added during the MoS_2 crystal formation may occupy these vacancies during exfoliation and improve the electrical performance of the MoS_2 FET, as can be observed from the transfer characteristics of the RT and 77 K samples. In relation to the crystal quality, samples 2 and 4 show high crystal quality, despite the large crystal size of the samples. The low cooling rates of 2 °C h^{-1} could make the material of sample 3 polycrystalline [15], which degrades the drain current of the device, but a high concentration of sulphur helps to heal these vacancies; thus, the current in sample 4 is higher than that in sample 3 but lower than that in sample 2. All four samples show an $I_{on/off}$ ratio of 10^6. A negative threshold voltage shift of −4.6 V is observed in sample 2. The transfer characteristics measured at 77 K (figure 3(b)) show thermally activated charge transport in all four devices, with a similar trend observed for the RT measured devices. This thermally activated charge transport is attributed to the hopping mechanism caused by defect-induced localized states, where the carriers are pinned within the specialised locations of these disorders which are either vacancies or some interstitial states. However, pinned carriers located near the Fermi level gain thermal energy and hop to their nearest neighbours by thermally activated hopping, or hop further to other locations, subject to an energy minimization constraint, in the variable-range hopping mode. This causes a negative temperature dependence of the mobility. The observed phenomenon is similar to the results reported by Ghatak *et al* for MoS_2 grown on SiO_2 [31]. Furthermore, this also can be realised in terms of a Schottky transition within the device due to the grain boundaries; however, the Schottky transition is quite untraceable in these devices, except for sample two, as depicted in figure 3(b). It is also noted that thermally activated trap charges also cause a shift in the threshold voltage of multilayer MoS_2 devices [32]. The threshold voltage shift and change in contact resistance are both visible in figure 3(b), which confirms the presence of thermally activated transport in all four devices. The threshold voltage increases towards the positive side with an increase in the drain current for all four samples. The field-effect mobilities for devices measured at RT and 77 K were extracted from the measured

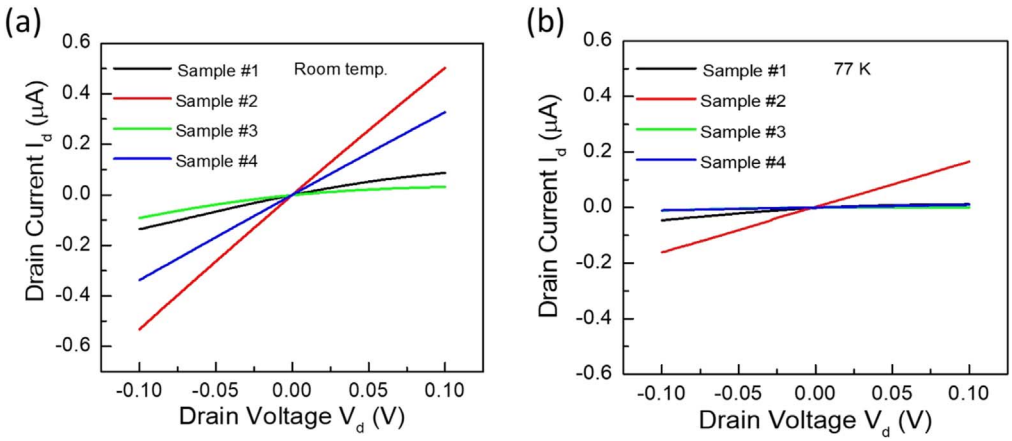

Figure 4. Output characteristics of the MoS_2 FET. (a) I_{ds} versus V_{ds} curve measured at room temperature for four different samples. (b) The I_{ds} versus V_{ds} curve measured at 77 K. Both measurements were carried out with a zero gate voltage. All measurements were carried out at 2×10^{-3} Torr of pressure.

Table 2. Comparisons of the electrical parameters for samples 1 to 4. The six-day growth process uses the 2.5 °C h^{-1} cooling rate, while the eight-day process uses the 2.0 °C h^{-1} cooling rate.

Sample name	Molecular ratio (Mo:S:Sn)	$I_{on/off}$ ratio	Threshold voltage (V_{th}) in (V)	Mobility (μ) in ($cm^2\ V^{-1}\ s^{-1}$)
		Room temperature		
Sample #1	1:2:15	10^6	−4.3	27.3
Sample #2	1:2.2:15	10^6	−4.6	45.1
Sample #3	1:2:15	10^6	2.3	16.5
Sample #4	1:2.2:15	10^6	−0.9	44.5
		77 K		
Sample #1	1:2:15	10^6	5.4	54.2
Sample #2	1:2.2:15	10^6	3.4	88.4
Sample #3	1:2:15	10^6	13.4	25.0
Sample #4	1:2.2:15	10^6	7.9	86.9

conductance (g_{max}) using the following equation [30]:

$$\mu = \left(\frac{L}{W}\frac{g_{max}}{C_{ox}V_{ds}}\right) \quad (1)$$

where g_{max} is the maximum peak value of dI_{ds}/dV_{gs}. A maximum room temperature mobility of 45.1 $cm^2\ V^{-1}\ s^{-1}$ was calculated for sample 2; while a field-effect mobility of 88.4 $cm^2\ V^{-1}\ s^{-1}$ was calculated for sample 2 at 77 K. The observed mobility is in good agreement with the mobility reported by Lin *et al* [33] for a five-layer MoS_2 (110 $cm^2\ V^{-1}\ s^{-1}$) FET non-h-BN device at 77 K measured at 10^{-6} Torr pressure. It is worth noting that the field-effect mobility is sensitive to the external environment. In this study, all measurements at 77 K were carried out at a 2×10^{-3} Torr of base pressure. Therefore, the extracted mobility is highest at this pressure at RT and 77 K, which to the best of our knowledge, reflects the best quality single-crystal formation of sample 2 with a 2.5 °C h^{-1} cooling rate. Unlike a monolayer MoS_2, the increase in field-effect mobility at low temperature is also assisted by the reduction in phonon scattering at low temperatures, because the multi-layered MoS_2 favours weaker phonon-electron interactions due to reduced lattice vibrations [34]. Table 2 shows the summary of all the calculated electrical parameters at RT and 77 K for MoS_2 FET devices grown via the flux method. Figures 4(a) and (b) show the output characteristics (I_{ds} versus V_{ds}) with no applied back-gate voltage (V_{gs}) for samples 1–4, characterized at room temperature and 77 K, respectively.

The linear behaviour with increasing applied drain voltage reflects the good ohmic contact between the exfoliated MoS_2 and the Au/In metal contact device and shows the strong dependence of the output drain current on the crystal morphology of the fabricated devices. The highest I_{ds} values were observed in samples 2 and 4 in figure 4, which displayed a strong dependency on the crystal quality similar to that discussed previously. Meanwhile, the output characteristics measured at 77 K in figure 4(b) show a deviation from the linear behaviour and a significant reduction in the drain current for all three samples, with the exception of sample 2.

Further, a transition from ohmic behavior for a Schottky barrier was observed for lower temperatures, which can be attributed to the grain boundary impurities in the samples grown under different conditions. These grain boundaries allow for a metal charge injection within the channel material at lower temperatures [35]. However, this metal injection can be improved at lower pressures close to approximately

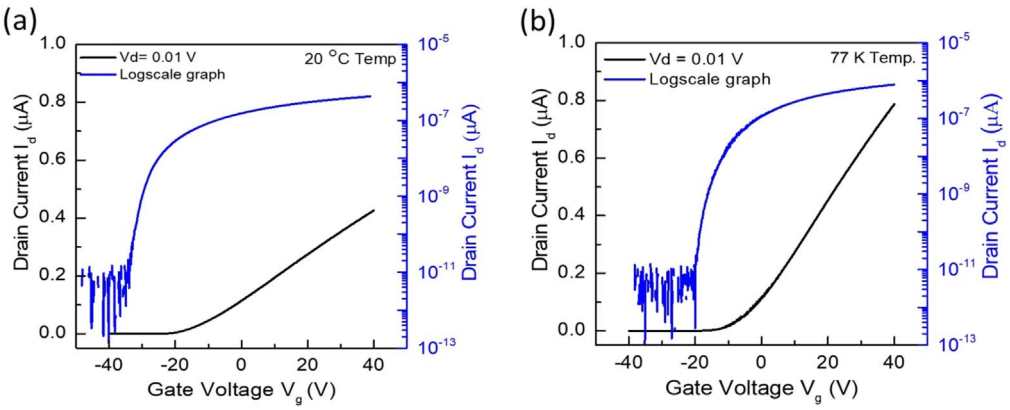

Figure 5. Electrical properties of the MoS_2/h-BN FET. (a) Id-Vg characteristics at room temperature with $V_{ds} = 0.01$ V and back-gate voltages varying from −40 V to 40 V. (b) I_d-V_g characteristics at 77 K with $V_{ds} = 0.01$ V and gate voltages ranging from −40 V to 40 V. All measurements were carried out at 2×10^{-3} Torr of pressure.

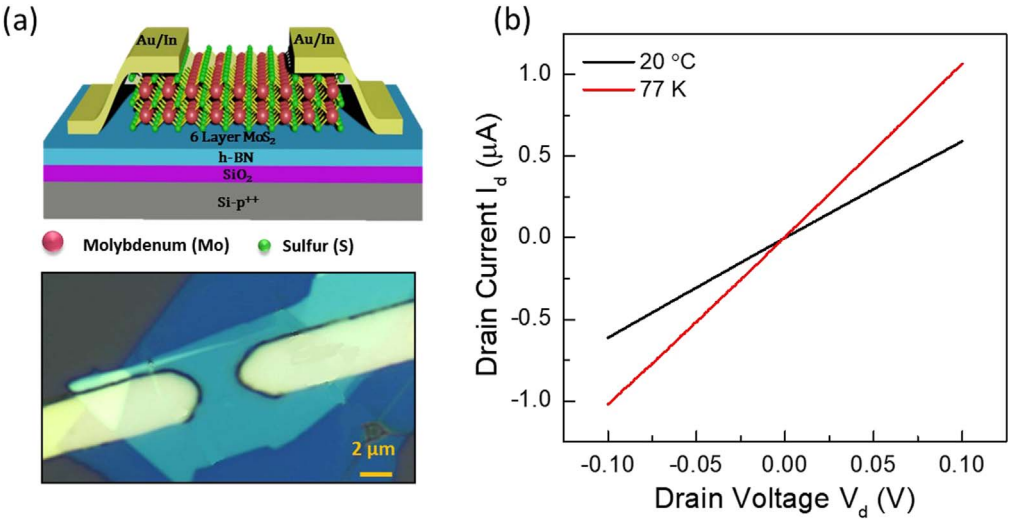

Figure 6. (a) Shows the device schematic and an optical device image of the real device. (b) I_{ds} versus V_{ds} curves of the MoS_2/h-BN FET measured at room temperature and 77 K. Both measurements were carried out at a zero gate voltage. All measurements were carried out at 2×10^{-3} Torr of pressure.

Table 3. A comparison of the electrical parameters for samples 1 to 4.

Device structure	Measurement conditions	$I_{on}/_{Off}$ ratio	Threshold voltage (V)	Mobility $cm^2\ V^{-1}\ s^{-1}$
MoS_2	RT	10^6	−4.6	45.1
	77 K	10^6	3.4	88.4
MoS_2/h-BN	RT	10^5	−23.16	50.5
	77 K	10^5	−10.54	113

10^{-6} Torr or by encapsulating the MoS_2 channel material using high-k dielectrics such as HfO_2 [36].

The transfer characteristics when h-BN is inserted as a dielectric layer between the SiO_2 and MoS_2 layers show high mobility (sample 2) among the four samples, as shown in figure 5. Figure 5(a) shows the measurements performed at RT and the 77 K measurements are shown in figure 5(b). As expected, both the room temperature and 77 K measurements show an improvement in the drain current with the insertion of few layers of h-BN between the MoS_2 and the SiO_2, compared to that of the non-h-BN MoS_2/SiO_2 FET. The insertion of the h-BN helps to improve the interface quality of 2D TMDs and SiO_2, and this improvement therefore enhanced the electric field of the device and the drain current.

Figure 6(a) shows a device schematic and an optical device image of the MoS_2/h-BN device; figure (b) shows the output characteristics of the MoS_2/h-BN FET device measured at RT and 77 K.

The hexagonal boron nitride (h-BN) layer is less rough than the SiO_2 surface and has no surface doping effect, resulting in improved mobility. The field-effect mobility was extracted for devices using equation (1). The device measured

at RT had a mobility of 50.5 $cm^2 V^{-1} s^{-1}$, while the highest mobility of 113 $cm^2 V^{-1} s^{-1}$ was achieved at 77 K at a pressure of 2×10^{-3} torr. Table 3 compares the electrical properties of the MoS_2 FETs with and without h-BN.

4. Conclusions

The effect of crystal morphology on the electrical properties of six-layer MoS_2 FETs was investigated. The Sn flux method was adopted to grow high-quality single-crystal MoS_2 material. The optical images confirm the variations in the crystal dimensions for different cooling rates, while the Mo and S molar ratio helps to modify the crystallinity. The Raman shift was used to verify the number of layers of exfoliated MoS_2 on SiO_2/Si. Room-temperature and low-temperature (77 K) measurements were carried out to investigate the electrical properties of the fabricated FET devices. The electrical properties revealed the great impact of crystal morphology on device performance. High-quality crystals with small grain boundaries and defects were obtained at a higher sulphur concentration and a cooling rate of 2.5 °C h^{-1}, showing an improvement in the field-effect mobility. Furthermore, the addition of few layers of h-BN improves the mobility significantly, as discussed. Our study shows that the flux method is effective in achieving crystal growth; in addition, the crystal quality of MoS_2 can be tuned by varying the molar ratio between Mo and S and the cooling rate during the growth process. Moreover, high-quality crystals with the addition of an h-BN dielectric could be the key to achieving higher mobility in MoS_2-based FET devices.

Acknowledgments

This work was supported by the National Research Foundation of Korea (NRF) grant funded by the Korea government (MSIT) (No. 2019R1A2C2088719, 2021K2A9A2A08000168, and 2012R1A3A2048816). N A acknowledges the support of the JSPS KAKENHI via grant number 18H01812. K W and T T acknowledge the support of the Elemental Strategy Initiative conducted by the MEXT, Japan, grant number JPMXP0112101001, JSPS KAKENHI grant number JP20H00354 and the CREST (JPMJCR15F3), JST.

Data availability statement

The data that support the findings of this study are available upon reasonable request from the authors.

ORCID iDs

Jihyun Kim https://orcid.org/0000-0002-1748-9223
Khushabu Agrawal https://orcid.org/0000-0001-8464-2104
Junsin Yi https://orcid.org/0000-0002-6196-0035
Nobuyuki Aoki https://orcid.org/0000-0001-9203-6040
Kenji Watanabe https://orcid.org/0000-0003-3701-8119
Gil-Ho Kim https://orcid.org/0000-0002-5153-4235

References

[1] Kuc A, Zibouche N and Heine T 2011 Influence of quantum confinement on the electronic structure of the transition metal sulphide TS_2 *Phys. Rev.* B **83** 245213
[2] Lee I *et al* 2016 Gate-tunable hole and electron carrier transport in atomically thin dual-channel WSe_2/MoS_2 heterostructure for ambipolar field-effect transistors *Adv. Mater.* **28** 9519
[3] Shi J *et al* 2014 Controllable growth and transfer of monolayer MoS_2 on Au foils and its potential application in hydrogen evolution reaction *ACS Nano* **8** 10196
[4] Khan K, Khan A T, Aslam M, Wang R, Zhang Y, Mahmood A, Ouyang Z, Zhang H and Guo Z 2020 Recent developments in emerging two-dimensional materials and their applications *J. Mater. Chem.* C **8** 387
[5] Li J and Ostling M 2015 Scalable fabrication of 2D semiconducting crystals for future electronics *Electronics* **4** 1033
[6] Tao L, Chen K, Chen Z, Chen W, Gui X, Chen H, Li X and Xu J-B 2017 Centimetre-Scale CVD growth of highly crystalline single-layer MoS_2 film with spatial homogeneity and the visualization of grain boundaries *ACS Appl. Mater. Interfaces* **9** 12073
[7] Zhao Y and Jin S 2020 Controllable water vapour assisted chemical vapour transport synthesis of WS_2-MoS_2 heterostructure *ACS Mater. Lett.* **2** 42
[8] Pisoni A, Jacimovic J, Barisic O S, Walter A, Nafradi B, Bugnon P, Magrez A, Berger H, Revay Z and Forro L 2015 The role of transport agents in MoS_2 single crystals *J. Phys. Chem.* C **119** 3918
[9] Siegel G, Subbaiah Y P V, Prestgard M C and Tiwari A 2015 Growth of centimetre-scale atomically thin MoS_2 films by pulsed laser deposition *APL Mater.* **3** 056103
[10] Zabinski J S, Donley M S, John P J, Dyhouse V J, Safriet A J and Mcdevitt N T 1991 Crystallization of molybdenum disulfide films deposited by pulsed laser ablation *MRS Online Proc. Libr.* **201** 195
[11] Mandyam S V, Kim H M and Drndic M 2020 Large area few-layer TMD film growths and their applications *J. Phys.: Mater.* **3** 024008
[12] Ly T H *et al* 2014 Observing grain boundaries in CVD-Grown monolayer transition metal dichalcogenides *ACS Nano* **8** 11401
[13] Kataria S, Wagner S, Cusati T, Fortunelli A, Iannaccone G, Pandey H, Fiori G and Lemme M C 2017 Growth-induced strain in chemical vapour deposited monolayer MoS_2: experimental and theoretical investigation *Adv. Mater. Interfaces* **4** 1700031
[14] Edelberg D *et al* 2019 Approaching the intrinsic limit in transition metal diselenides via point defect control *Nano Lett.* **19** 4371
[15] Zhang X *et al* 2015 Flux method growth of bulk MoS_2 single crystals and their application as a saturable absorber *Cryst. Eng. Comm.* **17** 4026
[16] Cevallos F A *et al* 2019 Liquid salt transport growth of single crystals of the layered dichalcogenides MoS_2 and WS_2 *Cryst. Growth Des.* **19** 5762
[17] Tsai M L *et al* 2014 Monolayer MoS_2 hetero-junction solar cells *ACS Nano* **8** 8317
[18] Lig L *et al* 2020 Magnetic plasmon resonances in nanostructured topological insulators for strongly enhanced light–MoS_2 interactions *Science & Applications* **9** 191

[19] Wang Y *et al* 2020 Difference frequency generation in monolayer MoS_2 *Nanoscale* **12** 19638
[20] Li L H *et al* 2015 Dielectric screening in atomically thin boron nitride nanosheets *Nano Lett.* **15** 218
[21] Illarionov Y Y *et al* 2016 The role of charge trapping in MoS_2/SiO_2 and MoS_2/hBN field-effect transistors *2D Mater.* **3** 035004
[22] Lee G H *et al* 2013 Flexible and transparent MoS_2 field-effect transistors on hexagonal boron nitride-graphene heterostructures *ACS Nano* **7** 7931
[23] Kim J H, Kim T H, Lee H, Park Y R, Choi W and Lee C J 2016 Thickness-dependent electron mobility of single and few-layer MoS_2 thin-film transistors *AIP Adv.* **6** 065106
[24] Nam D, Lee J U and Cheong H 2015 Excitation energy dependent Raman spectrum of $MoSe_2$ *Scientific Report* **5** 17113
[25] Qian Q, Zhang Z and Chen K J 2018 *In situ* resonant raman spectroscopy to monitor the surface functionalization of MoS_2 and WSe_2 for High-k integration: a first-principles study *Langmuir* **34** 2882
[26] Mahdavi M, Kimiagar S and Abrinaei F 2020 Preparation of few-layered wide bandgap MoS_2 with nanometer lateral dimensions by applying laser irradiation *Crystals* **10** 164
[27] Thangavel N K, Chandrasekaran N and Phani K L 2015 Structural and electronic modification of MoS_2 nanosheets using S-doped carbon for efficient electrocatalysis of the hydrogen evolution reaction *Chem. Commun.* **51** 5052
[28] Ye G, Gong Y, Lin J, Li B, He Y, Pantelides S T, Zhou W, Vajtai R and Ajayan P M 2016 Defects engineered monolayer MoS_2 for improved hydrogen evolution reaction *Nano Lett.* **16** 1097
[29] Han S W, Cha G-B, Kim K and Hong S C 2019 Hydrogen interaction with a sulfur-vacancy induced occupied defect state in the electronic band structure of MoS_2 *Phys. Chem. Chem. Phys.* **21** 15302
[30] Khan M A, Rathi S, Yun S J and Kim G-H 2020 Study of oxygen plasma induced modulation of photoconductivity in MoS_2 field effect transistor *Superlattice Microst.* **142** 106507
[31] Ghatak S, Pal A N and Ghosh A 2011 Nature of electronic states in atomically thin MoS_2 field-effect transistors *ACS Nano* **5** 7707
[32] Park Y, Baac H W, Heo J and Yoo G 2016 Thermally activated trap charges responsible for hysteresis in multilayer MoS_2 field-effect transistors *Appl. Phys. Lett.* **108** 083102
[33] Rathi S *et al* 2015 Tunable electrical and optical characteristics in monolayer graphene and few-layer MoS_2 heterostructure devices *Nano Lett.* **15** 5017
[34] Lin M-W, Kravchenko I I, Fowlkes J, Li X, Puretzky A A, Rouleau C M, Geohegan D B and Xiao K 2016 Thickness-dependent charge transport in few-layer MoS_2 field-effect transistors *Nanotechnology* **27** 165203
[35] Ahn J-H, Parkin W M, Naylor C H, Charlie Johnson A T and Drndic M 2017 Ambient effects on electrical characteristics of CVD-grown monolayer MoS_2 field-effect transistors *Sci. Rep.* **7** 4075
[36] Xu J, Wen M, Zhao X, Liu L, Song X, Lai P-T and Tang W-M 2018 Effects of HfO_2 encapsulation on electrical performances of few-layered MoS_2 transistor with ALD HfO_2 as back-gate dielectric *Nanotechnology* **29** 345201